Check for updates

JOURNAL OF THERMOPLASTIC COMPOSITE MATERIALS

Original Manuscript

Journal of Thermoplastic Composite Materials
1–20
© The Author(s) 2020
Article reuse guidelines:
sagepub.com/journals-permissions
DOI: 10.1177/0892705720953193
journals.sagepub.com/home/jtc
SAGE

Multi material 3D printing of PLA-PA6/TiO_2 polymeric matrix: Flexural, wear and morphological properties

Sudhir Kumar[1], Rupinder Singh[2,3], Mohit Singh[3], TP Singh[1] and Ajay Batish[1]

Abstract

The poly-lactic acid (PLA), bio compatible polyamide (PA6) and TiO_2 has established biomedical applications especially in 3D printing of scaffolds. But hitherto little has been reported on improving the performance of multi-material matrix for PLA-PA6/TiO_2 especially in 3D printing application of biomedical scaffolds. The anti-bacterial properties of PA6/TiO_2 make it worthy to be explored with PLA matrix in multi layered fashion on the platform of fused deposition modeling (FDM) being low cost 3D printing technology for in house development of scaffolds. In this work an effort has been made for in-house development of feedstock filaments of PLA and PA6/TiO_2 based polymeric composite matrix on twin screw extrusion (TSE) machine. Further the feedstock filament wires were used on FDM to establish the flexural, wear and morphological properties of multi-material 3D printed functional prototype. The results of the study suggest that for flexural strength, infill speed: 90mm/s; infill pattern: triangular and layer combination as 5 consecutive layers of PLA and 5 consecutive layers of PA6/TiO_2 are the optimized conditions for FDM printing. The wear testing results suggest that the composite of PA6/TiO_2 held low wear rate (823 μm) in comparison to PLA (wear rate: 1092 μm). Further porosity testing (based upon optical photomicrographs) at ×100 and fractured surface analysis at ×30 supported the observed trends for flexural and wear testing. The photomicrographs of fractured surface were 3D rendered to predict the role of surface roughness (Ra) profile for flexural properties. The mechanical and morphological

[1] Department of Mechanical Engineering, Thapar Institute of Engineering and Technology, Patiala, Punjab, India
[2] Department of Mechanical Engineering, National Institute of Techanical Teachers Training and Research, Chandigarh, India
[3] Department of Production Engineering, Guru Nanak Dev Engg. College, Ludhiana, Punjab, India

Corresponding author:
Rupinder Singh, Department of Mechanical Engineering, National Institute of Technical Teachers Training and Research, Chandigarh, India; Department of Production Engineering, Guru Nanak Dev Eng. College, Ludhiana 141006, Punjab, India.
Email: rupindersingh@nitttrchd.ac.in

observations are also supported with scanning electron microscopy (SEM) and energy-dispersive X-ray spectroscopy (EDS) analysis.

Keywords
Flexural strength, wear track, frictional force, porosity testing, fractured surface analysis, polyamide, poly(lactic acid)

Introduction

The reinforcement of fillers (in terms of fiber/powder) into thermoplastic matrix induces valuable enhancement in physicochemical and mechanical properties of thermoplastics.[1] At present, different types of fillers are reinforced in order for enhancement of one or more mechanical properties such as tensile, compressive, flexural, pull-out strength etc..[2] It has been reported that nano particle reinforcements offers new technological and economic benefits. The reinforcement of nano particles as reinforcement (e.g. nanofibre, nanotubes and layered silicates of clay and metal nanoparticles in polymeric materials) significantly has improved the mechanical properties of base polymer.[3] Nano powder of TiO_2 is one the oldest and most conventional agents for the purpose of self-cleaning, antibacterial, UV blocking substrate, catalytic, purification, and optoelectronic devices.[4–9] Variety of polymers (such as thermoplastics, thermoset, functional polymers, composites, and hydrogels) has been used extensively in additive manufacturing. For enhancement of mechanical properties of polymeric blends while using 3D printing technology it has been established that the input process parameter parameters (like mechanical properties, build speed, surface finish and accuracy etc.) played vital role hence, the process parameters need to be optimized for selected polymeric composite.[8] The advancements in 3D printing materials (such as thermoplastics: PLA, PA6, acrylonitrile butadiene styrene (ABS), etc.) has helped in enhancing the scope of FDM process.[10,11] The mechanical and water barrier properties were improved with the blending of PA6 in polypropylene (PP).[12] PA6 has been established as a good barrier against oxygen but has shown poor resistance to water and water vapor. On the contrary, PP exhibits excellent moisture barrier, which has helped in enhancement of water resistance property of PA6.[13] FDM process parameter (such as: Infill density, infill speed, building orientation, infill pattern and temperature condition) influences the mechanical properties of 3D printed specimens.[14] Layer thickness and infill density has shown enhancement in mechanical properties of the 3D printed functional prototype.[15] The process parameters (such as built orientation, layer thickness and fiber volume content) have significant impact on the mechanical properties of 3D printed specimens of fiber reinforce composite. The layer thickness and number of perimeter for 3D printed object in case of PA6 functional prototypes have increased the tensile and flexural strength significantly.[16] The mechanical properties for polymeric composite has been observed to be increased with 3D printing at low infill angle (0°) and high infill density (100%) than high infill angle and low infill density. The 3D printed virgin PLA sample printed at 0° orientation of

nozzle has shown better tensile strength (105 MPa) than sample printed at 45° orientation angles.[17]

For in-house development of feedstock filament of new polymeric composite the twin screw extrusion (TSE) machine has been widely used with reinforcement of metallic / non-metallic /ceramic fillers in polymer matrix. The various process parameters (such as: material composition; rotational speed of TSE; die temperature of TSE; particle grain size and applied load on TSE) are mainly used for the preparation of feed stock filaments.[18] Better feeding and more positive conveying characteristics of TSE prepared filament with uniform distribution of fillers as compared to single-screw extruders have been widely reported.[19] The process parameters of TSE have significant impact on tensile characteristics of reinforced polymer. TSE has brought a revolution in material extrusion because of uniform blending of suitable proportions of different ingredients in thermoplastic granules.[20] There is significant effect of size of reinforcement in polymeric matrix as researchers have observed higher flexural modulus with the addition of nanofillers in comparison to virgin thermoplastic. Also, with increase in filler percentage in polymeric matrix the water intake capacity of the thermoplastic nano-composites has been found to be enhanced. The nano-composite containing carbon nano-tubes exhibited better water absorption capabilities.[21] The increasing load of PA6 wt% in the composite has shown significant improvement in flexural properties of polymeric matrices.[22] The Kenaf-bamboo-coir/PLA composites reinforcement increases the mechanical strength approximately 20 to 78% higher than bamboo-coir/PLA and Kenaf coir/PLA reinforcement respectively. But the Young's modulus of the three composites was obtained ranging from 6.0 to 7.5 GPa.[23] Researchers have widely explored the impact of different input parameters (such as: layer density, thickness, speed, infill perimeter and extrusion temperature) on maximum value of flexural force in PLA specimen.[24] The reinforcement of 4 wt% organoclay in polymeric matrix has shown better mechanical properties than other reinforcement levels of organoclay in polymer thus it was observed that with higher loading of organoclay there was drop in both strength and strain values.[25]

From literature review it has been ascertained that researchers have focused on FDM printing of polymeric matrix by introducing foreign fillers in the basic matrix of polymer for different applications such as structural, non structural, medicinal application but hitherto little has been reported on flexural, wear and morphological properties of multi-material specimens of PLA and PA6/TiO_2. Therefore present investigation deals with primary objective of (i) development of flexural functional prototype of PLA-PA6/TiO_2 composite using in-house developed feedstock filament and secondary objective of (ii) optimization of FDM processing parameters and exploration of flexural, wear and morphological properties of multi-material composite matrix through UTM, Wear testing, porosity testing, photo-micrographic image analysis.

Materials and methods

For this study PLA was procured from local supplier (Shiva chemicals limited, Ludhiana, India) and PA6/TiO_2 composite was procured from lab of (Dr. Fernando Fraternali, Professor, Dept. of Civil Engineering) University of Salerno, Italy. The procured

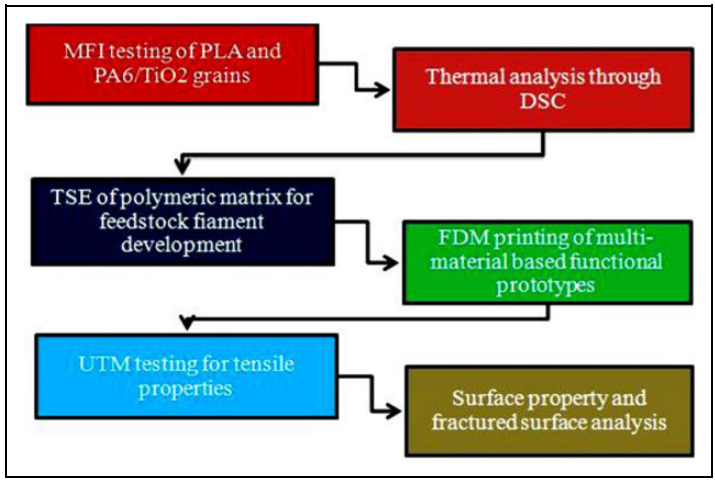
MFI testing of PLA and PA6/TiO2 grains
Thermal analysis through DSC
TSE of polymeric matrix for feedstock fiament development
FDM printing of multi-material based functional prototypes
UTM testing for tensile properties
Surface property and fractured surface analysis

Figure 1. Methodology used for optimization of printing conditions for flexural specimens.

Table 1. Mechanical property of PLA and PA6/TiO_2.

Material-matrix/Properties	PLA[26]	PA6/TiO_2[27]
Tensile Strength	59 MPa	62.6 MPa
Young Modulus	1280 MPa	532 MPa
Elongation at Break	7%	13.35%

polymers were in granule form therefore the procured polymers were processed with TSE machine and feedstock filament of standard dimension 1.75 $\pm$ 0.05 mm was prepared in-house for FDM processing. Figure 1 shows the methodology used for present investigation. Table 1 shows the mechanical properties of basic polymeric matrix of PLA and PA6/TiO_2.

Experimentation

FDM printing of multi-material functional prototypes

The extrusion of polymers was performed using TSE machine (Model: Haake, Germany) using barrel temperature 250°C, load 10 kg and screw rotation of 90 rpm. The developed feedstock filaments were used for FDM printing (FDM model: Accuraft 250D, Divide by Zero) of flexural specimens. The FDM with single nozzle facility was used for current investigation by manually changing the feed stock filament material at required time. An open source slicing software (Slicer 3r) package tool was used for present investigation and 3D printing of functional prototype on FDM platform. For 3D printing of flexural specimen ASTM D790 standard was used. Figure 2a shows the ASTM D790 specification for design of functional prototype and Figure 2b shows the standard testing

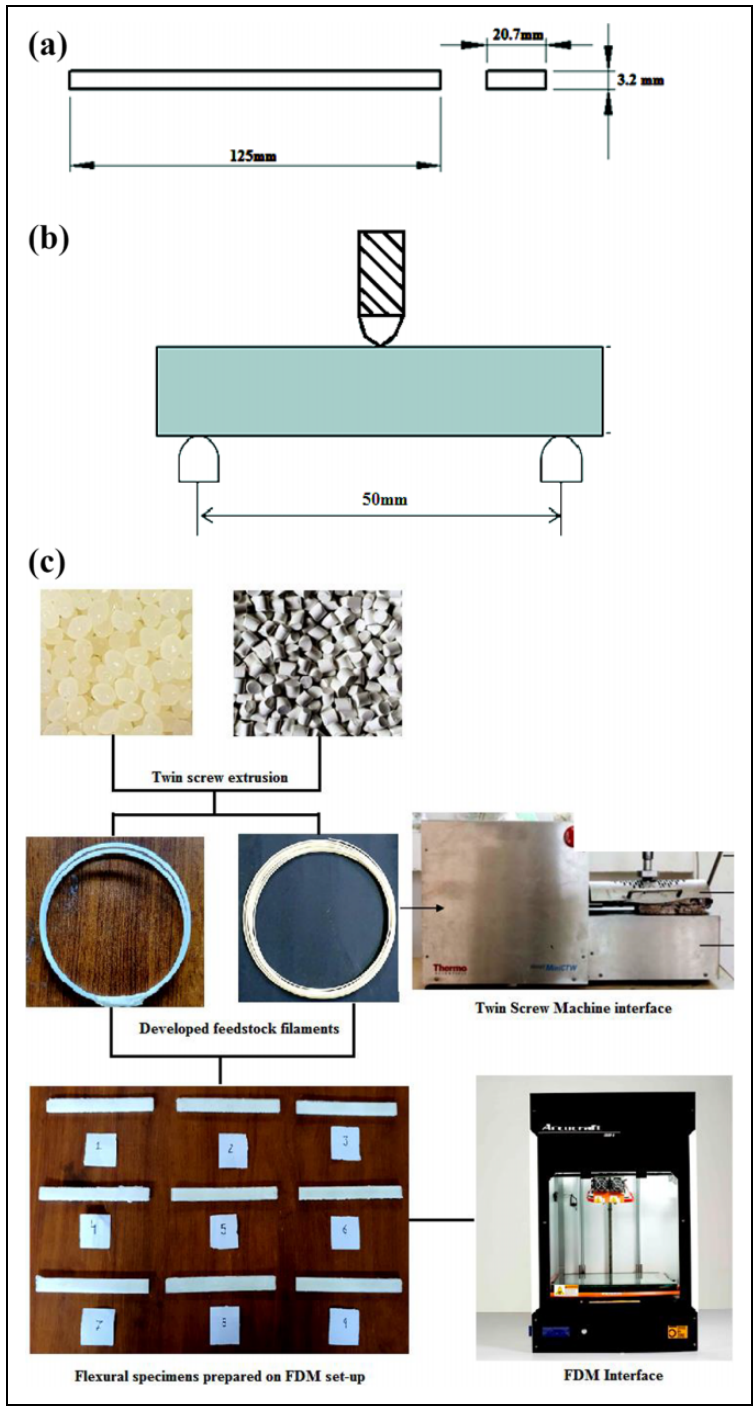

Figure 2. (a) Flexural functional prototype design as per ASTM D790 standard, (b) standard testing condition and (c) systematic approach for development of flexural specimen.

Table 2. DOE with layer combination representation.

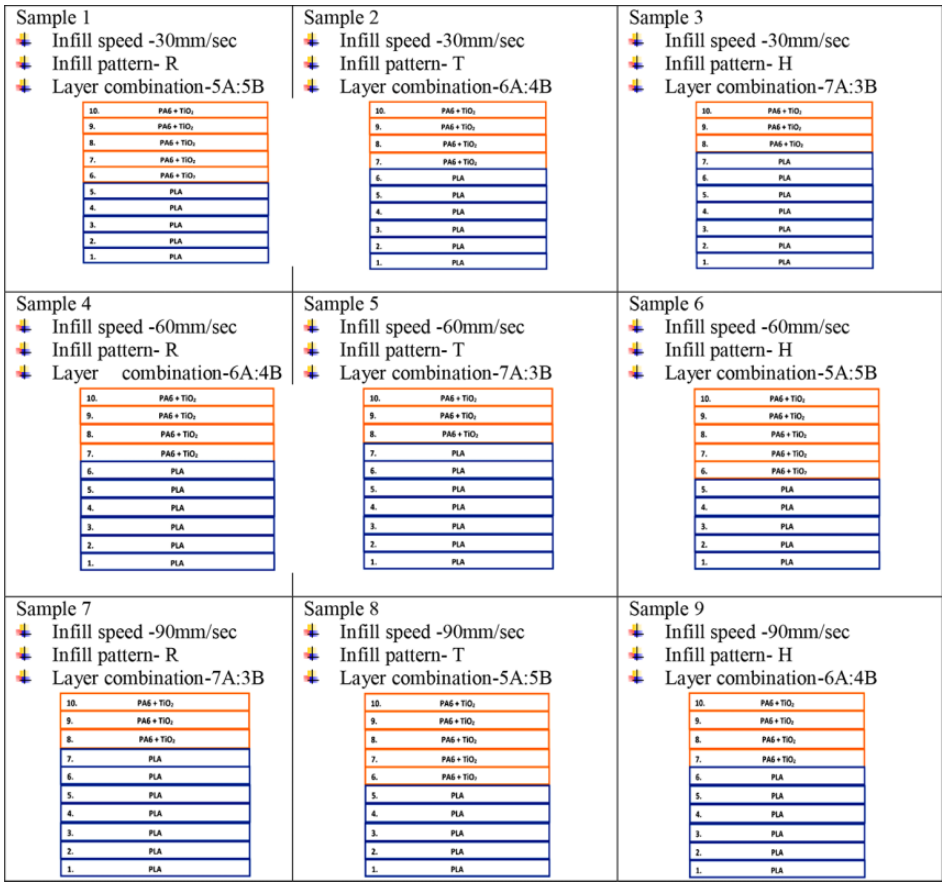

Note:

(1): Infill pattern as: R: Rectilinear, T: Triangle, H: Honeycomb

(2): Layer combination of PLA (A), PA6/TiO_2(B) as: 5A:5B, 6A:4B and 7A:3B based upon the fact that total 10 number of layers were printed for flexural samples according to standards of ASTM D790

conditions for flexural functional prototype.[28] Taguchi L9 orthogonal array (OA) methodology was used to optimize the printing conditions. Table 2 shows the design of experiment (DOE) for present investigation as per Taguchi L9 orthogonal array (O.A) and Figure 2c shows the systematic approach for conversion of polymeric grains of PLA and PA6/TiO_2 into FDM printed flexural specimens. From literature review of FDM work it has been ascertained that infill speed, infill angle, infill pattern, nozzle diameter, and material selection plays important role in functional prototype performance. Therefore in this study three of the variable input parameters of FDM (Infill speed, infill pattern and layer combination) were chosen while other parameters may have significant contribution toward the mechanical properties of FDM printed prototype. The reason

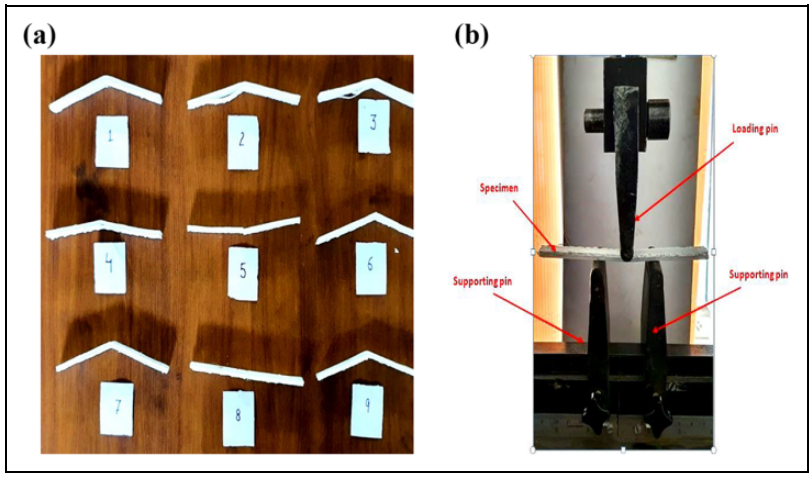

Figure 3. Flexural tested 3D printed functional prototype and (b) flexural testing set up.

behind selecting only three combination of PLA-PA6/TiO_2 (5:5, 6:4 and 7:3) was based on the MFI as the MFI of PLA was approx 27 g/(10 min) and forPA6/TiO_2 was approx (56g/(10 min) due to which the PA6/TiO_2 matrix held low thickness on solidification in comparison to PLA for the same layer height through nozzle. Therefore for optimum thickness of functional prototype less number of layers was selected for PA6/TiO_2 in single multi-material prototype.

UTM testing

The developed flexural functional prototypes were subjected to UTM testing according to ASTM D790 standard (see Figure 2b). The UTM machine (Make: Shanta engineering limited, Pune, India) for flexural testing was of 5000 N capacity and the samples were tested at uniform speed of testing 30mm/min. Figure 3a and 3b respectively show the UTM setup used for flexural testing and destructed samples after flexural testing.

Wear property testing

To compare the wear properties of selected composite matrix of PLA and PA6/TiO_2 wear testing was performed using wear pins prepared on moulding machine. The pins were prepared of equal size ϕ80 mm. After developments of polymeric pins the pins were loaded on wear testing setup specifically known as Pin on disc (Make: Ducom, Hyderabad, India). The wear testing conditions were selected as weight: 0.5 kg, rotation speed: 71 rpm and time for testing: 2 min. Figure 4 shows the pin on disc setup. For wear testing total six pins (three of PLA (100 wt %) and three of PA6/TiO_2 (70/30 wt %)) were tested and average value for wear and frictional force was observed.

Figure 4. Pin on disc setup.

Table 3. Flexural results of PLA-PA6-TiO_2 (as per Table 2).

S.No.	PL (N)	BL(N)	FSP (MPa)	FSB (MPa)
1	175.0 ± 2.0	157.5 ± 2.5	78.9 ± 1.5	70.9 ± 1.5
2	109.3 ± 1.5	98.4 ± 2.0	49.3 ± 1.0	44.3 ± 1.0
3	153.4 ± 1.5	138.1 ± 1.5	69.1 ± 1.0	62.2 ± 1.5
4	131.4 ± 1.0	118.3 ± 1.0	59.2 ± 1.0	53.3 ± 1.5
5	186.8 ± 2.0	168.1 ± 2.0	84.2 ± 1.5	75.8 ± 1.0
6	193.6 ± 2.0	174.2 ± 2.0	87.3 ± 1.5	78.5 ± 1.2
7	201.5 ± 2.0	181.3 ± 2.0	90.8 ± 1.5	81.7 ± 1.4
8	212.8 ± 2.5	191.5 ± 2.0	95.9 ± 2.0	86.3 ± 2.0
9	141.7 ± 1.8	127.5 ± 1.5	63.9 ± 1.0	57.5 ± 1.5

Note: PL: Peak load, BL: Break load, FSP: Flexural strength at peak, FSB: Flexural strength at break. Three samples for each experiment were fabricated using FDM printer with provided DOE (as per Table 2). Three repetitions were made to reduce the experimental error

Morphological testing

For morphological analysis the flexural tested samples were analyzed for morphological properties such as porosity and photo-micrographic analysis of fractured surface. For porosity testing metallurgical image analysis software (MIAS) package was used and photomicrographs were taken at ×100 using ASTM B276 standard of testing. For fractured surface analysis Tool maker's microscope was used and images were taken at ×30. It should be noted that the morphological properties were observed at fractured surface of tested functional prototype.

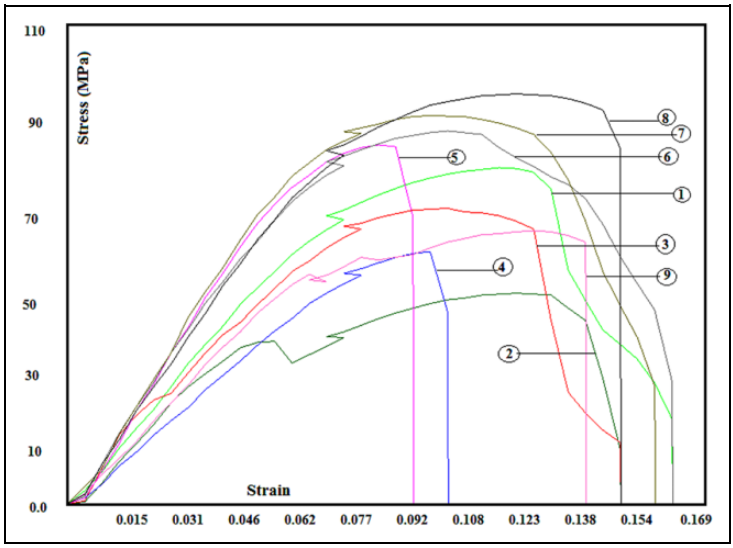

Figure 5. Stress vs. strain diagram for flexural tested specimen (as per Table 1).

Result and discussions

UTM testing results

The flexural specimens of PLA-PA6-TiO_2 have shown compatibility for FDM printing as the flexural specimens of different layer combination of functional prototypes were successfully 3D printed. The 3D printed samples were tested for flexural properties such as peak strength and break strength. Table 3 shows the flexural testing results (based upon Table 2). Three samples for each experiment were fabricated using FDM printer with provided DOE (as per Table 2). The average value for each experiment trail was calculated and was quoted in Table 3. The standard deviation for each experiment was also calculated and was given with the average value of flexural properties (see Table 3). The maximum flexural strength at peak (FSP) of 95.91 MPa was observed for sample no. 8 which was prepared with Infill speed: 90mm/s, infill pattern: triangular and layer combination of 5A:5B (A: PLA, B: PA6/TiO_2) FDM printing conditions. To optimize the printing conditions of FDM, analysis of variance (ANOVA) has been used. Figure 5 shows the stress vs. strain diagram for flexural samples. As observed from Table 3 relatively better mechanical properties were noticed for sample at S.No. 8 and poor for sample at S.No. 2. Also the area under stress-strain curve (Figure 5) was more for sample at S.No. 8, hence it is ascertained that modulus of toughness will be more for this sample, which may be particularly useful for impact resistance in typical scaffolding applications. Further based upon Table 3, signal to noise (SN) ratio was calculated for maximum the better type case and mean effect plots were drawn (Figure 6). As observed from Figure 6; infill speed; 90mm/s, infill pattern: rectilinear and layer combination of 5A:5B was the optimum FDM processing conditions. It has been observed that the sample 8

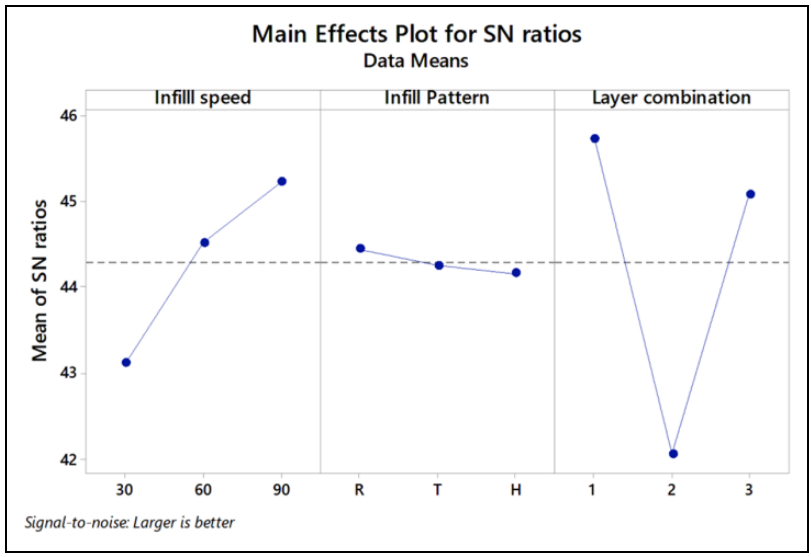

Figure 6. Main effect plot for SN ratio of peak load for flexural specimen.

Table 4. ANOVA results for SN ratios.

Source	DF	Seq SS	Adj SS	Adj MS	F	P	% contribution
Infill speed	2	6.89	6.89	3.44	64.21	0.015	22.93
Infill Pattern	2	0.12	0.12	0.06	1.13	0.470	0.40
Layer combination	2	22.94	22.94	11.47	213.59	0.005	76.31
Residual Error	2	0.10	0.10	0.05			
Total	8	30.06					

DF: Degree of freedom, Seq SS: Sequential sum of square, Adj SS: Adjusted sum of square, F: Fisher's value, P: Probability

which has shown maximum flexural strength was printed with triangular pattern but the optimized condition has recommended rectilinear pattern. To ascertain the reason ANOVA analysis was conducted for PL (Table 4), from which it was observed that layer combination has played maximum role. It was observed that the maximum percentage (%) contribution (76.31%) for flexural property was given by layer combination and second largest contribution for flexural property was given by infill speed (22.93% contribution). Table 5 shows the rank table for SN ratio of PL from which it was observed that layer combination has been given rank 1, infill speed at 2nd rank and infill pattern has been raked at 3 rd position (with just 0.4% contribution). The experimental condition 5, 4 and 9 have shown least strain capacity (approx 0.092, 0.108 and 0.138 respectively) in which it was observed that the sample no. 4 and 9 held large porosity value which resulted into poor strain capacity and mechanical properties whereas in case

Table 5. Rank table for SN ratio of peak load.

Level	Infill speed	Infill pattern	Layer combination
1	43.12	44.44	45.72
2	44.51	44.25	42.06
3	45.22	44.16	45.08
Delta	2.11	0.28	3.66
Rank	2	3	1

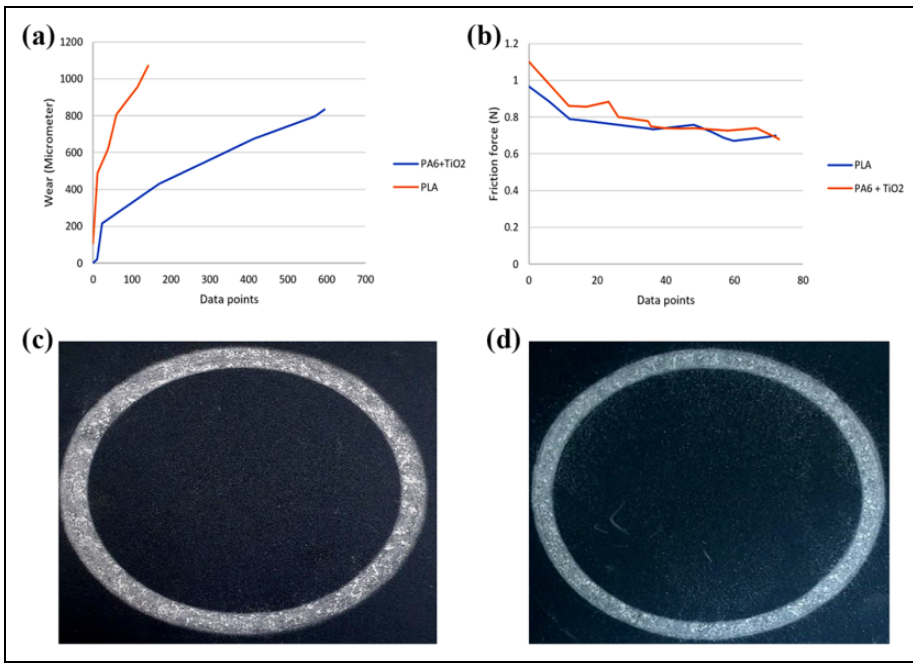

Figure 7. (a). Wear rate graph, (b) Coefficient of friction graph, (c) wear track for PLA pin, (d) wear track for PA6/TiO_2.

of sample 5 the composite held 7A:3B (PLA: PA6/TiO2) composition in which large PLA presence has made composition brittle due to which the strain capacity got reduced.

Further the rank table values have been used for optimization of peak load value to know the optimized printing condition.

$$X\,\text{opt} = l + (\text{lA} - 1) + (\text{lB} - 1) + (\text{lC} - 1) \tag{1}$$

$$G^2_{\text{opt}} = 10^{X\,\text{opt}/10}(\text{for properties, larger is better case}) \tag{2}$$

w = SN mean of PL = 44.28, lA = max infill speed from Table 5 = 45.22, lB = max infill pattern from Table 5 = 44.44, lC = layer combination value from Table 5 = 45.72

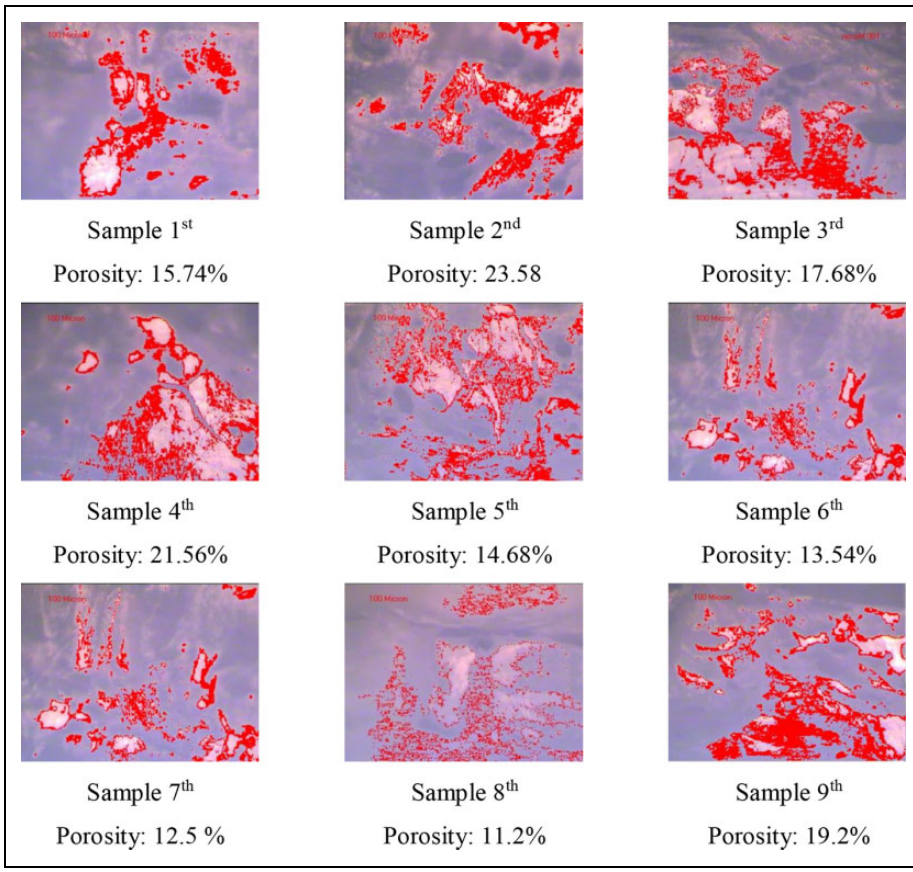

Figure 8. Porosity testing graphs for flexural specimens (as per Table 2).

Putting all values in equation (1)

$$X\text{opt} = 44.28 + (45.22 - 44.28) + (44.44 - 44.28) + (45.72 - 44.28)$$

$$X\text{opt} = 46.82\,\text{dB}$$

$$G_{\text{opt}}^2 = 1046.82/10$$

$$G_{\text{opt}} = 219.28\ N$$

Thus it can be observed that the optimized value (219.8 N) for the peak load was very near to the value of peak load for sample no. 8. Therefore the printing conditions for sample no. 8 may be considered as the optimized condition for flexural specimens of multi-material component of PLA-PA6/TiO_2.

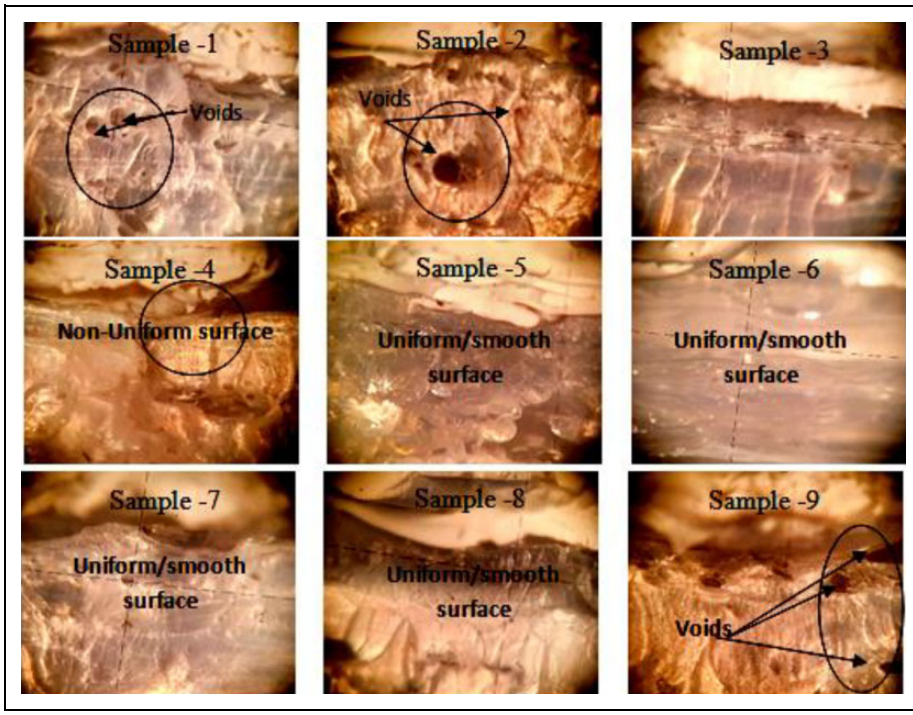

Figure 9. Tool maker's microscopic photo-micrograhs (as per Table 2) 3D rendered image Surface roughness profile of fractured sample.

Wear testing results

From wear testing it has been observed that PLA material has shown highest wear rate (1092 μm) in compare to PA6/TiO_2 (823 μm) while the coefficient of friction was approximate equal for both of the sample. This may be due to the reason that PA6 has higher bonding strength than PLA which resulted into low wear rate of PA6-TiO_2 composite sample. Figure 7a shows the wear rate graph for PLA and PA6/TiO_2 pin from which it was observed that wear graph of PLA was large and for PA6/TiO_2 the wear graph has moved upto 823 μm. Figure 7b shows the graph of coefficient of friction from which it may be observed that the coefficient of friction for both sample was 0.7 N. Figure 7c which shows the wear tracks of PLA and Figure 7d for PA6/TiO_2 from which it may be observed that the wear track impression was more for PLA which gave evidence of higher wear of PLA. Wear testing was performed on circular pins of PLA-PA6/TiO_2 based composite prepared on moulding machine. From wear testing it has been observed that PLA held high wear rate in comparison to PA6/TiO_2 thus in situations where wear rate has high significance then there will be top layering of PA6/TiO_2. But in most of the cases of biomedical scaffold application the PA6/TiO_2 material matrix will always be inside as PA6/TiO_2 needs to be in touch with skin as it possesses anti bacterial properties.

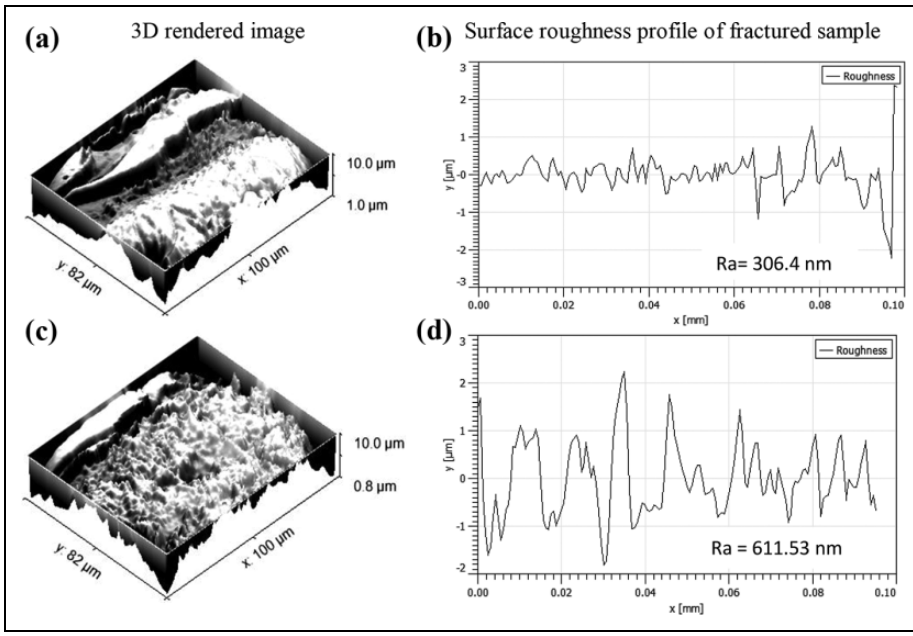

Figure 10. (a) 3D rendered image of sample no. 8, (b) Ra profile for sample no. 8, (c) 3D rendered image of sample no. 2, (d) Ra profile for sample no. 2.

Morphological property results

Porosity testing results. The photomicrographs of porosity testing have shown clear opposite trends for morphological and mechanical properties of multi-material based specimens (Figure 8). It was observed from the porosity results that the sample no. 8 which held best flexural property held least relative porosity value (11.2%) whereas the sample no. 2 held large porosity value. Hence from porosity analysis it was ascertained that the mechanical performance is inversely related to the sample porosity. This may be due to the fact that large porosity holes/ voids inside the 3D printed components resulted into poor bonding of intra and inter layer semisolid material layer which was ultimately incapable of producing better mechanical performance. The results are in-line with the previous studies.[29–33] The high porosity values were observed for sample no 2, 4 and 9 (23.58, 21.56 and 19.2% respectively) which existed for 6:4 (PLA: PA6/TiO_2) layer combination. The trends were in-line with the flexural result as for sample 2, 4 and 9 the flexural peak strength was less (49.26, 59.22 and 63.87 MPa respectively). Thus it was clear that there was negative relation between mechanical and morphological properties such as for the samples with poor mechanical properties there was high porosity.

Photo-micrographic investigation of fractured surface. From photo-micrographic image of Tool maker's microscope it was observed that the sample with better mechanical performance had less number of void/porosity holes on fractured surface. Figure 9 shows

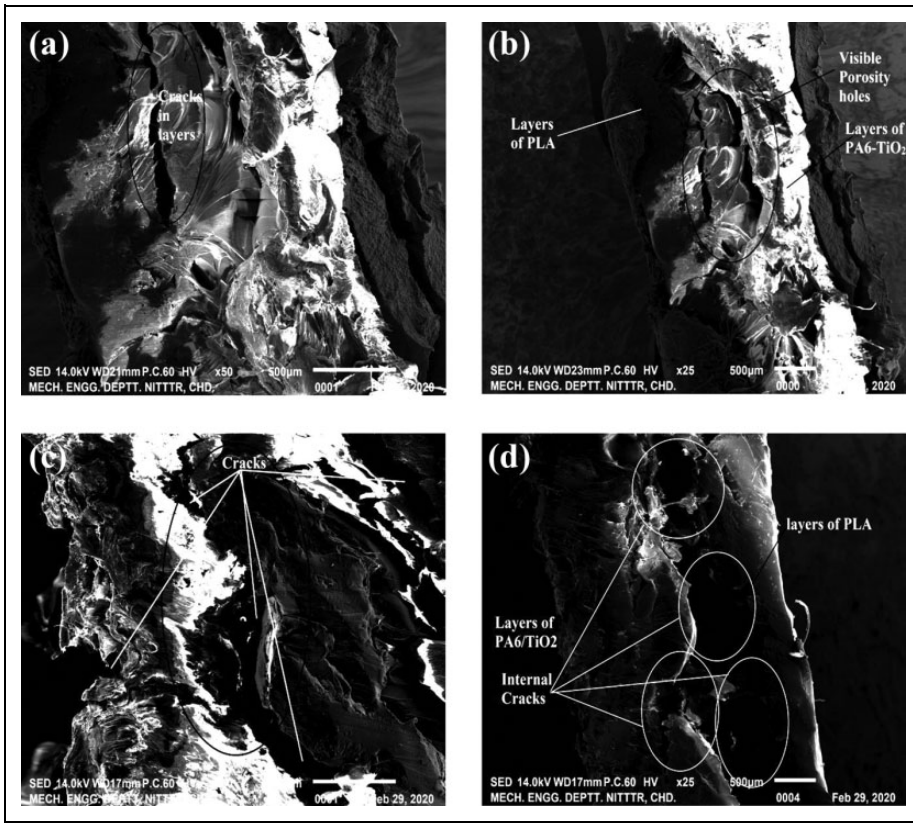

Figure 11. SEM image for (a) sample no. 8 at ×50, (b) sample no. 8 at ×25, (c) sample no. 2 at 50 and (d) sample no. 2 at ×25.

the photomicrographs at fractured surface of specimen at ×30 magnification. It was observed that the sample no. 8 held uniform/smooth surface which was indication of better mechanical strength. The results are in line with previous studies.[34–36] The photomicrographic images taken by Tool maker's microscope for sample no. 8 and sample no. 2 was processed using 3D rendering software package tool (Figure 10) to analyze the Ra profile of best (sample no. 8) and worst sample as per mechanical performance (sample no. 2). The cut off length of 0.05 mm was selected for 3D rendering of images. From Ra profile it was observed for sample no. 8 the Ra value was 306.4 nm which is less than the Ra value of sample no. 2 (611.53 nm), hence counter verifies that the large porosity holes present inside the component resulted into large surface roughness of sample no. 2 and thus ultimately poor mechanical properties.

SEM and EDS analysis results. The Figure 11a to d shows the results for SEM analysis from which it was observed that the material settled while solidification in different layers have internal cracks which means that the PLA and PA6/TiO_2 were not fully

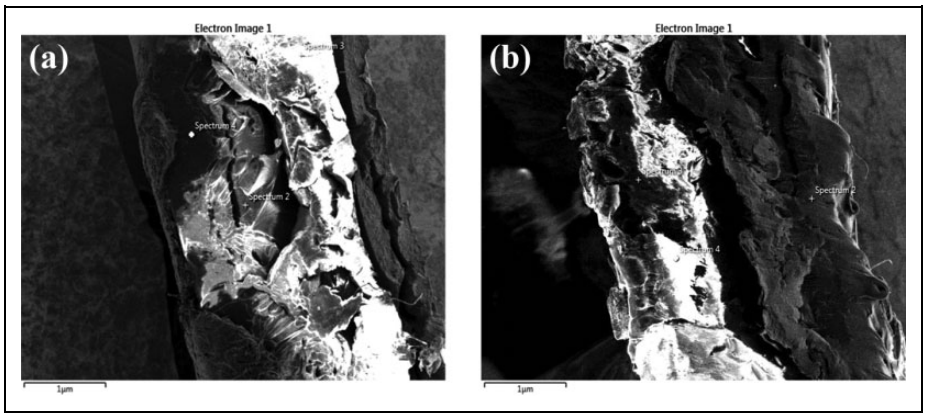

Figure 12a. EDS image spectrum selection over the entire region of (a) sample no. 8 and (b) sample no.2.

compatible with each other. The same can also be seen from their flexural testing results (Figure 9). In flexural tested samples the images have shown extirpation of layers or pulling out of layers of PLA and PA6/TiO_2. From the SEM images of sample no. 8 (Figure 11a and b) and sample no. 2 (Figure 11c and d) it was clear that more internal cracks were present for sample 2 which resulted into poor joining of material layers and ultimately poor flexural strength of 3D printed samples. Figure 12a and 12b shows the EDS results for sample no. 8 and sample no. 2 respectively. From Figure 12a it was observed that maximum TiO_2 (12.10%) (See Appendix 1 (Table 1A EDS result for sample no. 8)) was observed in spectrum 1 of selected region which was right side of the spectrum selected as the spectrum moved toward left there was no presence of TiO_2 which means toward right side there was only presence of PLA layers. From Figure 12b it was observed that sample no. 2 also held 11–12% of TiO_2 ((See Appendix 1 (Table 2A EDS result for sample no. 2)) in spectrum 1 and 2 thus the proportion of PA6-TiO_2 for best and poor samples were almost equal which meant that the internal structure (level of cracks/ voids among the deposited layers) of the samples played vital role in their flexural properties.

Conclusions

The present investigation deals with primary objective of (i) development of flexural functional prototype of PLA-PA6/TiO_2 composite using in-house developed feedstock filament and secondary objective of (ii) optimization of FDM processing parameters and exploration of flexural, wear and morphological properties of multi-material composite matrix through UTM, Wear testing, porosity testing, photo-micrographic image analysis. Following are the outcomes from the present study:

From the investigation it can be concluded that the selected multi-material composite design is feasible and the functional prototype were successfully prepared.

From process optimization of FDM it may be concluded that infill speed of 90mm/s, infill pattern of rectilinear and layer combination of 5A:5B are the optimized printing conditions for flexural components.

The wear testing has made it clear that the material PA6/TiO_2 held less material wear in comparison to PLA; hence PA6/TiO_2 based specimens may be used for high wear rate applications.

Morphological testing (porosity, fractured surface analysis and 3D rendering) has clearly supported the observed trends of flexural properties and have shown that the samples with higher porosity/ voids resulted into higher Ra and ultimately lower flexural properties.

From SEM and EDS analysis, it has been ascertained that the internal cracks/ voids present in deposited layers of 3D printed functional prototypes played vital role in flexural strength of specimens.

Future scope

The present work is limited to only three input variable of FDM as the main focus of the study was on investigating the flexural properties of new multi-material composite design of PLA-PA6/TiO_2. Therefore further studies may be taken to explore the effect of different input variable on PLA-PA6/TiO_2 based multi-material composite design, where several input parameters of FDM may also be taken at once by choosing different DOE and analysis approach. Multi-nozzle FDM may be used further to study the effect of delay in case of manual change of feedstock and automatic change of feedstock on properties of composite.

Acknowledgements

The authors are highly thankful to Professor Fernando Fraternali (University of Salerno, Italy), Thapar Institute of Engineering and Technology (TIET), National Institute of Technical Teacher Training and Research (NITTTR) and manufacturing research lab of Guru Nanak Dev Engineering College for their continuous technical support.

Funding

The author(s) received no financial support for the research, authorship, and/or publication of this article.

ORCID iDs

Sudhir Kumar https://orcid.org/0000-0001-7636-1564
Rupinder Singh https://orcid.org/0000-0001-8251-8943
Mohit Singh https://orcid.org/0000-0002-5097-8272

References

1. Wilches LV, Uribe JA and Toro A. Wear of materials used for artificial joints in total hip replacements. *Wear* 2008; 265(1-2): 143–149.

2. Samyn P, Quintelier J, Schoukens G, et al. The sliding behaviour of sintered and thermoplastic polyimides investigated by thermal and Raman spectroscopic measurements. *Wear* 2008; 264(9-10): 869–876.
3. Magalhães LC, Volpato N and Luersen MA. Evaluation of stiffness and strength in fused deposition sandwich specimens. *J Braz Soc Mech Sci Eng* 2014; 36(3): 449–459.
4. Kumar N, Jain PK, Tandon P, et al. Extrusion-based additive manufacturing process for producing flexible parts. *J Braz Soc Mech Sci Eng* 2018; 40(3): 143.
5. Soni A, Kumar S and Singh B. Prediction of tensile strength of 3D printed part using response surface methodology. *J Braz Soc Mech Sci Eng* 2018; 40(12): 566.
6. Bhalodi D, Zalavadiya K and Gurrala PK. Influence of temperature on polymer parts manufactured by fused deposition modeling process. *J Braz Soc Mech Sci Eng* 2019; 41(3): 113.
7. Rajpal R, Lijesh KP and Gangadharan KV. Experimental investigation of 3D-printed polymer-based MR sandwich beam under discretized magnetic field. *J Braz Soc Mech Sci Eng* 2018; 40(12): 569.
8. Foster HA, Ditta IB, Varghese S, et al. Photocatalytic disinfection using titanium dioxide: spectrum and mechanism of antimicrobial activity. *Appl Microbiol Biot* 2011; 90(6): 1847–1868.
9. Singh R, Kumar R, Pawanpreet, et al. On mechanical, thermal and morphological investigations of almond skin powder-reinforced polylactic acid feedstock filament. *J Thermoplast Compos Mater*. Epub ahead of print 5 November 2019. DOI: 10.1177/0892705719886010.
10. Singh R and Ranjan N. Experimental investigations for preparation of biocompatible feedstock filament of fused deposition modeling (FDM) using twin screw extrusion process. *J Thermoplast Compos Mater* 2018; 31(11): 1455–1469.
11. Holsti-Miettinen RM, Perttilä KP, Seppälä JV, et al. Oxygen barrier properties of polypropylene/polyamide 6 blends. *J appl polym sci* 1995; 58(9): 1551–1560.
12. Kojima Y, Usuki A, Kawasumi M, et al. Sorption of water in nylon 6-clay hybrid. *J Appl Polym Sci* 1993; 49(7): 1259–1264.
13. Popescu D, Zapciu A, Amza C, et al. FDM process parameters influence over the mechanical properties of polymer specimens: a review. *Polym Test* 2018; 69: 157–166.
14. Torres J, Cotelo J, Karl J, et al. Mechanical property optimization of FDM PLA in shear with multiple objectives. *JOM* 2015 67(5), 1183–1193.
15. Chacón JM, Caminero MA, Núñez PJ, et al. Additive manufacturing of continuous fibre reinforced thermoplastic composites using fused deposition modelling: effect of process parameters on mechanical properties. *Compos Sci Technol* 2019; 181: 107688.
16. Letcher T and Waytashek M. Material property testing of 3D-printed specimen in PLA on an entry-level 3D printer. In: *ASME 2014 international mechanical engineering congress and exposition*, Montreal, Quebec, Canada, 14–20 November 2014. American Society of Mechanical Engineers Digital Collection, 2014; 46438: V02AT02A014.
17. Singh R and Ranjan N. Experimental investigations for preparation of biocompatible feedstock filament of fused deposition modeling (FDM) using twin screw extrusion process. *Journal of Thermoplastic Composite Materials* 2018; 31(11): 1455–1469.
18. Rauwendaal C. *Polymer extrusion*. Munich: Carl Hanser Verlag GmbH Co KG, 2014.
19. Singh R, Singh S, and Hashmi MS. Polymer twin screw extrusion with filler powder reinforcement. In: *Reference Module in Materials Science and Materials Engineering*, 2017. DOI: 10.13140/RG.2.2.27553.30560.
20. Chou PM, Mariatti M, Zulkifli A, et al. Evaluation of the flexural properties and bioactivity of bioresorbable PLLA/PBSL/CNT and PLLA/PBSL/TiO2 nanocomposites. *Compos Part B Eng* 2012; 43(3): 1374–1381.

21. Li J. Flexural properties of blends of polyamide 6 with PTFE. *Materials Technology* 2009; 24(4): 236–239.
22. Yusoff RB, Takagi H and Nakagaito AN. Tensile and flexural properties of polylactic acid-based hybrid green composites reinforced by kenaf, bamboo and coir fibers. *Industrial Crops and Products* 2016; 94: 562–573.
23. Luzanin O, Guduric V, Ristic I, et al. Investigating impact of five build parameters on the maximum flexural force in FDM specimens—a definitive screening design approach. *Rapid Prototyp J* 2017; 23(6): 1088–1098.
24. Chow WS, Ishak ZM, Ishiaku US, et al. The effect of organoclay on the mechanical properties and morphology of injection-molded polyamide 6/polypropylene nanocomposites. *J Appl Polym Sci* 2004; 91(1): 175–189.
25. Kumar S, Singh R, Singh TP, et al. On investigation of rheological, mechanical and morphological characteristics of waste polymer-based feedstock filament for 3D printing applications. *J Thermoplast Compos Mater*. Epub ahead of print 11 June 2019. DOI: 10.1177/0892705719856063.
26. Farah S, Anderson DG and Langer R. Physical and mechanical properties of PLA, and their functions in widespread applications—a comprehensive review. *Advanced drug delivery reviews* 2016; 107: 367–392.
27. Soundararajan R, Jayasuriya N, Vishnu RG, et al. Appraisal of mechanical and tribological properties on PA6-TiO2 composites through fused deposition modelling. *Mater Today* 2019 18, 2394–2402.
28. Kumar S, Singh R, Singh TP, et al. Flexural, pull-out, and fractured surface characterization for multi-material 3D printed functionally graded prototype. *J Composit Mater* 2020; 54: 2087–2099.
29. Kumar S, Singh R, Singh TP, et al. Investigations of polylactic acid reinforced composite feedstock filaments for multimaterial three-dimensional printing applications. *P I Mech Eng Part C: J Mech Eng Sci* 2019 233(17), 5953–5965.
30. Kumar S, Singh R, Singh TP, et al. Investigations for magnetic properties of PLA-PVC-Fe3O4-wood dust blend for self-assembly applications. *J Thermoplast Compos Mater*. Epub ahead of print 20 June 2019. DOI: 10.1177/0892705719857778.
31. Kumar S, Singh R, Singh TP, et al. Multimaterial printing and characterization for mechanical and surface properties of functionally graded prototype. *P I Mech Eng Part C: J Mech Eng Sci* 2019; 233(19-20), 6741–6753.
32. Kumar S, Singh R, Singh TP, et al. On mechanical characterization of 3-D printed PLA-PVC-wood dust-Fe3O4 composite. *J Thermoplast Compos Mater*. Epub ahead of print 8 October 2019. DOI: 10.1177/0892705719879195.
33. Kumar S, Singh R, Singh TP, et al. (2019). PLA composite matrix as functional prototypes for four dimensional applications. In: Hashmi MSJ (ed.) *Reference Module in Material Science and Material Engineering*. Amsterdam: Elsevier, 2019, pp 1–10.
34. Kumar S, Singh R, Singh TP, et al. Additive manufacturing of smart materials exhibiting 4-D properties: a state of art review. *J Thermoplast Compos Mater*. Epub ahead of print 13 December 2019. DOI: 10.1177/0892705719895052.
35. Kumar S, Singh R, Singh TP, et al. (2017). Polymer waste as fused deposition modeling feed stock filament for industrial applications. In: Hashmi MSJ (ed.) *Reference Module in Material Science and Material Engineering*. Elsevier, 2017, pp. 1–12.
36. Kumar S, Singh R, Singh TP, et al. (2020). Investigations for mechanical, thermal and magnetic properties of polymeric composite matrix for four-dimensional printing applications. *J Braz Soc Mech Sci Eng* 2020; 42(4): 1–15.

Appendix 1

Table 1A. EDS analysis results for sample no. 8.

Spectrum 1		
Element	**Line Type**	**Weight %**
C	K series	48.63
O	K series	36.06
Ti	K series	12.10
Spectrum 2		
Element	**Line Type**	**Weight %**
C	K series	63.97
O	K series	36.03
Spectrum 3		
Element	**Line Type**	**Weight %**
C	K series	65.74
O	K series	34.26
Spectrum 4		
Element	**Line Type**	**Weight %**
C	K series	67.41
O	K series	32.59

Table 2A. EDS spectrum analysis for sample no. 2.

Spectrum 1		
Element	**Line Type**	**Weight %**
C	K series	51.12
O	K series	38.11
Ti	K series	11.22
Spectrum 2		
Element	**Line Type**	**Weight %**
C	K series	58.04
O	K series	31.50
Ti	K series	10.47
Spectrum 3		
Element	**Line Type**	**Weight %**
C	K series	80.14
O	K series	19.86
Spectrum 4		
Element	**Line Type**	**Weight %**
C	K series	63.28
O	K series	36.72